Density Functional Calculations of ATP Systems. 1. Crystalline ATP Hydrates and Related Molecules

ARTICLE *in* THE JOURNAL OF PHYSICAL CHEMISTRY B · MAY 2006

Impact Factor: 3.3 · DOI: 10.1021/jp054920l · Source: PubMed

2 AUTHORS, INCLUDING:

Jaakko Akola
Tampere University of Technology
97 PUBLICATIONS **2,896** CITATIONS

Density Functional Calculations of ATP Systems. 1. Crystalline ATP Hydrates and Related Molecules

J. Akola[†] and R. O. Jones*

Institut für Festkörperforschung, Forschungszentrum Jülich, D-52425 Jülich, Germany

Received: August 31, 2005; In Final Form: February 8, 2006

Adenosine 5′-triphosphate (ATP) is an essential energy carrier in mammalian and other cells, and its hydrolysis to the diphosphate (ADP) in the presence of metal cations (e.g., Mg^{2+} or Ca^{2+}) is one of the most prevalent biochemical reactions. We describe here density functional (DF) calculations on closely related systems and compare the results with other calculations and available experimental data: $Na(H_2O)_n^+$, $Mg(H_2O)_n^{2+}$, and $Ca(H_2O)_n^{2+}$ clusters ($n = 1, 4-7$), the crystalline pyrophosphates $Mg_2P_2O_7 \cdot 6H_2O$ and α-$CaNa_2P_2O_7 \cdot 4H_2O$, and crystalline $Na_2ATP \cdot 3H_2O$. The last of these comprises asymmetric units of ATP dimers (monomers A and B) in a double-protonated state $H_2(ATP)^{2-}$. The calculated structures agree well with available measurements and provide additional information, including the location of the H atoms. Analysis of the dipole moments of individual ATP monomers and their dimers shows that the crystal comprises blocks of opposing dipoles. Replacing one Na^+ ion with Mg^{2+} or Ca^{2+} results in a significant elongation of the terminal bridging P−O bond. The calculations provide benchmarks for the use of DF methods in ATP systems and are used in the companion paper to study the hydrolysis of ATP at the active site of the protein actin.

I. Introduction

Adenosine 5′-triphosphate (ATP) is essential to many biochemical processes, particularly in providing energy as a phosphorylating agent in cellular metabolism.[1] It comprises an adenine base, a ribose, and a strongly hydrophilic (charged) triphosphate; the adenosine portion can be viewed as a means of binding to enzymes or proteins, and the phosphate groups participate in energy capture. When energy stored in ATP is used, an environment-dependent hydrolysis results in adenosine diphosphate (ADP) and inorganic phosphate P_i. The reverse reaction is catalyzed, for example, by the enzyme ATP synthase. In his Nobel Prize address in 1997, Boyer estimated that the synthesis of ATP is the most prevalent chemical reaction in the human body. In fact, since plants and microorganisms capture and use energy by the same reaction, it is "the principal chemical reaction occurring in the whole world!"[2] Its obvious importance has resulted in countless studies.

The various components of ATP are neutral and charged, basic and acidic, and hydrophobic and hydrophilic, and its reaction with other biomolecules (proteins and enzymes) and with water is environment-dependent. ATP is then both a source of energy and a promoter of conformational change in biomolecules. The role of the proteins myosin and actin in muscle contraction and cellular motility shows the importance of such changes,[1] and many DNA-modifying enzymes consume ATP in an energetically unfavorable manner to maintain their genomic integrity.[3]

X-ray diffraction studies of proteins and enzymes have provided much information about ATP, but its properties depend on the environment, the presence of metal cations, its protonation state (pK_a), and the interactions with other molecules (hydrogen bonds, hydrophobic contacts, steric hindrance). Experimental data are also often analyzed using standard estimates of some structural parameters. Theoretical methods capable of predicting structures and their changes are of obvious value, and recent developments in hardware and algorithms have extended the range of applicability of density functional (DF) calculations to systems with hundreds of atoms, i.e., large enough to be relevant for the study of ATP and some neighboring molecules.

In earlier work we have modeled the ATP hydrolysis reaction (conversion of ATP complexed with Mg^{2+} to ADP and an inorganic phosphate P_i) in an aqueous environment.[4] We have also performed Monte Carlo calculations on a model designed to elucidate the polymerization of proteins (actin and tubulin) in the presence of ATP and guanosine triphosphate (GTP), respectively.[5] In neither case is direct structural information available from experiment, and we describe here DF calculations[6] on systems related to ATP for which such information is available from other calculations and X-ray diffraction measurements. We focus on ATP in crystalline phases and on the hydrated metal cations that play an important role in determining its properties. Experimental X-ray data are available for Na_2ATP hydrates and for ternary complexes composed of ATP, divalent cations, and aromatic heterocyclic amines.[7−10] A detailed comparison with experiment confirms the reliability of the DF approach, and structural details beyond those measured will aid the development of models of ATP-related systems.[5] In the companion paper we study the hydrolysis of ATP in the presence of the active site of the protein actin.

We describe the methods of calculation in section II. Results for hydrated cations of Na, Mg, and Ca [$Na(H_2O)_n^+$, $Mg(H_2O)_n^{2+}$, and $Ca(H_2O)_n^{2+}$ clusters ($n \leq 7$)] using three DF methods follow in section III, together with crystal structures of two pyrophosphates: $Mg_2P_2O_7$ hexahydrate and $Na_2CaP_2O_7$ tetrahydrate. We present DF results for Na_2ATP hydrates, which appear to be the only class of pure ATP crystal salts for which

* Author to whom correspondence should be addressed. E-mail: r.jones@fz-juelich.de.

[†] Present address: Nanoscience Center, Department of Physics, University of Jyväskylä, P.O. Box 35, Jyväskylä FI-40014, Finland.

10.1021/jp054920l CCC: $30.25
Published on Web 03/25/2006

X-ray diffraction data have been analyzed[11−13] and conclude in section IV.

II. Methods of Calculation

The Car−Parrinello molecular dynamics (CPMD) package[6] is used most extensively. The electron−ion interaction is described by a nonlocal, norm-conserving, and separable pseudopotential,[14] and semicore electrons for the metal cations Na^+, Mg^{2+}, and Ca^{2+} are included because there are ionic bonds between these metal ions and phosphate/water O atoms. Periodic boundary conditions (PBCs) are employed using a single point ($\mathbf{k} = 0$) in the Brillouin zone, and the approximation of Perdew, Burke, and Ernzerhof (PBE) is used for the exchange−correlation energy.[15] Increasing the kinetic energy cutoff (80 Ry for ATP crystal salts) to 100 Ry for smaller pyrophosphate crystals produces small changes in the bond lengths and angles of water molecules alone. This approach yields accurate results for the isolated H_3PO_4 molecule.[4]

We present results for clusters of metal cation hydrates calculated using two other DF programs. The hybrid CP2K method[16] uses analytic pseudopotentials,[17] and the valence electron orbitals and density are expanded in Gaussian-type functions and a plane wave auxiliary basis, respectively.[18] The use of the two basis sets leads to greater numerical efficiency than in the CPMD method. The Gaussian-type basis sets are double- and quadruple-ζ basis sets with *d*-polarization functions (DZVP, QZV3P). The plane wave auxiliary basis has a cutoff of 600 Ry for the density (corresponds to 150 Ry for the orbitals), and we use PBE and BLYP[19,20] functionals for the exchange correlation energy. The use of the pseudopotential approximation in these two methods has been checked against all-electron calculations[21] using a Gaussian-type basis set (DZVP, auxiliary basis A1). The PBE functional approximation is not available with this package, but the PW91 and PBE approximations generally lead to very similar results.[22]

III. Results

A. $Na(H_2O)_n^+$, $Mg(H_2O)_n^{2+}$, and $Ca(H_2O)_n^{2+}$ Clusters. We have performed calculations on $Na(H_2O)_n^+$, $Mg(H_2O)_n^{2+}$, and $Ca(H_2O)_n^{2+}$ clusters ($n = 1, 4-7$). Periodic boundary conditions are not used[23] in the CPMD calculations to avoid interaction between charged replicas, and the kinetic energy cutoff for plane waves was 100 Ry. The ionic positions are optimized using a quasi-Newton approach[24] and simulated annealing. Vibrational frequencies calculated using a linear response scheme were used to determine the zero-point energy (ZPE) corrections at 298 K.

The properties of cation−hydrate clusters are listed in Tables 1−4, and the optimized geometries are shown in Figure 1. For Na^+ mono- and hexahydrate there is good agreement between the three DF methods and MP2 results (Table 1). The CPMD result for the cation−oxygen distance is the shortest both for mono- and hexahydrate, but the overall variation (0.034 and 0.024 Å, respectively) is small. The hydration energies E_b for the monohydrate are close to the experimental values, but the ZPE-corrected value of $Na(H_2O)_6^+$ is underestimated, because the hexacoordinated isomer (6B, Figure 1) lies higher in energy than the tetracoordinated 6C, for which the hydration energy (93.8 kcal/mol) agrees better with experiment.

The effects of changing basis sets and exchange−correlation functional are evident in the results for $Mg(H_2O)^{2+}$ and $Mg(H_2O)_6^{2+}$ (Table 2). The Mg−O distances for mono- and hexahydrate lie within narrow ranges (0.039 and 0.027 Å, respectively). An MP2 study[25] with an extensive basis set reports a value (1.920 Å) for $Mg(H_2O)^{2+}$ in the center of this range. For $Mg(H_2O)_6^{2+}$ the distance (2.081 Å) is slightly shorter than the DF values. The ZPE corrections again bring the hydration energies closer to the MP2 result, with the exception of the BLYP calculation for the hexahydrate. The similarities between CPMD and CP2K/QZV3P results (both use extensive basis sets and the PBE functional) and the CP2K/DZVP and DGauss/DZVP results suggest that the differences in Table 1 are caused by the smaller basis set of DGauss not by the pseudopotential approximation or the PW91 functional. The CP2K/QZV3P calculations with PBE and BLYP functionals show no large deviations, although BLYP leads to a slightly longer cation−oxygen distance.

The DF results for $Ca(H_2O)^{2+}$ and $Ca(H_2O)_6^{2+}$ (Table 3) include results of a CPMD study using the BLYP functional.[26] Our Ca−O distance for the hexahydrate is 0.046 Å shorter. The DGauss result (2.403 Å) lies between these two values, and an MP2 study[27] reports a value of 2.39 Å (6-31+G* basis set). The Ca−O bond length is sensitive to the pseudopotential construction, and changes of 0.05 Å have been observed in Ca−O distances for different localized basis sets (B3LYP functional) with little change in hydration energy.[28]

The CPMD calculations yield slightly shorter cation−oxygen distances than the other DF methods (Tables 1−3), but the overall agreement with experiment and available MP2 data is very good. The overestimate of the O−H bond in water (0.01 Å, Table 2) is a familiar property of gradient-corrected functionals, although our calculation for free H_2O gives a bond angle of 104.3° (experimental value 104.5°). The H_2O geometries differ for different cations: for Mg^{2+} the elongation of the O−H bond and the opening of the H−O−H angle are more apparent than those for Na^+, and Ca^{2+} is intermediate. This effect is related to the charge transfer from H_2O to the cation and to the Coulomb repulsion between the protons and the cation.

As in earlier studies of water solvation of metal cations,[25−35] we assume that a full hydration shell of Na^+, Mg^{2+}, and Ca^{2+} accommodates 4, 6, and 6 water molecules, respectively. Several such structures (Figure 1) are shown in Table 4. The tetrahedral isomer of $Na(H_2O)_4^+$ (Figure 1, S_4 symmetry) and a C_s-conformation with a different orientation of water molecules have comparable hydrate binding energies E_b. The larger hydrates also prefer 4-fold coordination, and the most stable forms of $Na(H_2O)_5^+$ (5B) and $Na(H_2O)_6^+$ (6C) are found by adding one or two H_2O molecules to the outer hydration shell so that each forms two hydrogen bonds. We have also tested isomers based on the octahedral lowest-energy structures of $Mg(H_2O)_6^{2+}$ and $Ca(H_2O)_6^{2+}$ (6A). This form of sodium hexahydrate transforms spontaneously into a flat isomer (6B, S_6). Removal of one H_2O from the octahedral geometry yields two further pentacoordinated $Na(H_2O)_5^+$ isomers (5A and 5C) with very similar binding energies but different orientations of the atop water molecule. The pentacoordinated isomers 6D and 6F are related to the isomers 5A and 5C, respectively, and a pentacoordinated isomer (7C, C_2) is preferred for $Na(H_2O)_7^+$. This structure has a cyclic hydrogen-bond network in the lower half of the cluster and can be obtained by optimizing either 7A or 7B, both of which are stable for Ca^{2+}. A stable hexacoordinated structure for $Na(H_2O)_7^+$ (7D) is obtained by adding one H_2O molecule to isomer 6B.

Most structures for Mg^{2+} and Ca^{2+} are related to the octahedral isomer 6A, which is the most stable form of both hexahydrates, and stable structures for neighboring sizes (5A and 7B) were obtained by adding or removing one H_2O molecule. As in $Na(H_2O)_4^+$, both tetrahydrates prefer S_4

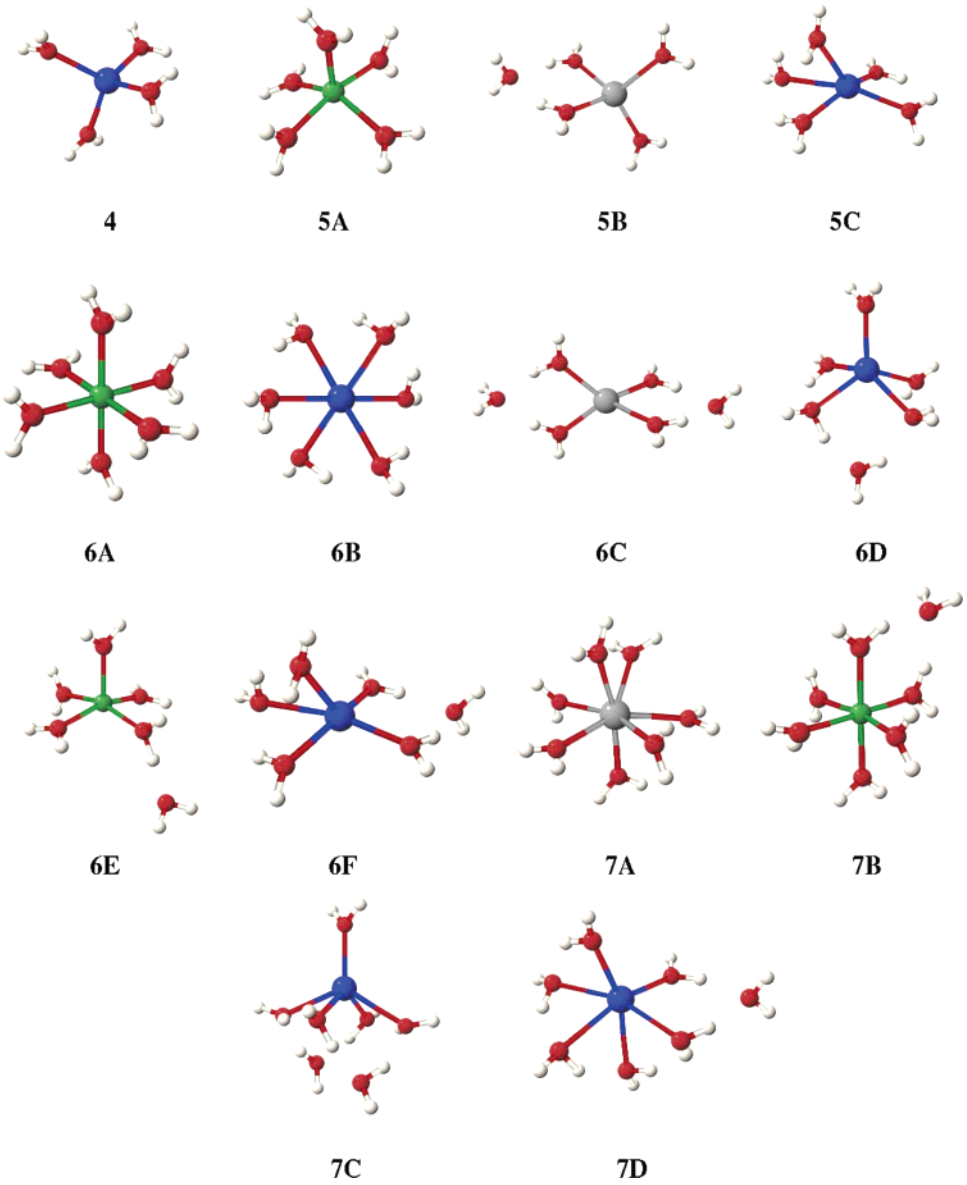

Figure 1. Calculated geometries of $Na(H_2O)_n^+$, $Mg(H_2O)_n^{2+}$, and $Ca(H_2O)_n^{2+}$ clusters. Color key: O, red; H, white; Na, blue; Mg, green; Ca, gray.

TABLE 1: Geometries and Hydrate Binding Energies of $Na(H_2O)^+$ and $Na(H_2O)_6^+$[a]

$Na(H_2O)_n^+$		CP2K/QZV3P[b]	DGauss[b]	CPMD[b]	MP2	expt[c]
1	r(Na−O)	2.227	2.238	2.204	2.21[d]	
	r(O−H)	0.972	0.980	0.971		
	α(H−O−H)	104.6	104.6	104.7		
	α(Na−O−H)	127.7	127.7	127.7		
	E_b	24.4 (22.8)	27.8 (26.2)	24.4 (22.8)	23.9[d], 23.8[e]	24.0
6	r(Na−O)	2.438	2.431	2.414	2.432[f]	
	r(O−H)	0.970, 0.978	0.978, 0.987	0.969, 0.980		
	α(H−O−H)	106.4	106.4	106.8		
	E_b	103.9 (90.3)	106.1 (92.5)	101.9 (88.3)	91.2[g]	96.4

[a] Hexacoordinated isomer, S_6 symmetry. Energies in kcal/mol, distances in angstroms, angles in degrees. [b] Values in parentheses include ZPE energy correction at 298 K. [c] Reference 36. [d] Reference 27, aug-cc-pVTZ basis set. [e] Reference 29, TZ3P basis set. [f] Reference 55, 6-311G(d,p) basis set. [g] Reference 30, 6-31+G* basis set.

symmetry, but the energy barrier for H_2O rotation is very small. Tetracoordinated motifs for larger hydrates (5B and 6C) are close in energy to the most stable isomer. (In $Mg(H_2O)_6^{2+}$ the binding energies of 6A and 6C differ by only 0.9 kcal/mol.) This is consistent with electrospray ionization measurements[35] of the dissociation rate constant of $Mg(H_2O)_6^{2+}$ as a function of temperature, which were explained by the coexistence of hexa- and tetracoordinated isomers. Starting from 6D of $Na(H_2O)_6^+$, we have optimized 6E for both Mg^{2+} and Ca^{2+}. Coulomb repulsion between the cation and the positively charged hydrogens of the external H_2O lead to this structure, in which hydrogen atoms point outward. The heptacoordinated geometry (7A) found for Ca^{2+} transforms spontaneously to isomer 7B for Mg^{2+}, which has a smaller ionic radius.

Table 4 shows calculated values of hydration energies E_b and successive water binding energies ΔE. A comparison with

TABLE 2: Geometries and Hydrate Binding Energies E_b of $Mg(H_2O)^{2+}$ and $Mg(H_2O)_6^{2+}$[a]

$Mg(H_2O)_n^{2+}$		CP2K/DZVP[b]	CP2K/QZV3P[b]	DGauss[b]	CPMD[b]	MP2[e]
1	r(Mg−O)	1.933	1.916[c], 1.929[d]	1.940	1.901	1.920
	r(O−H)	0.994	0.985[c], 0.989[d]	0.995	0.985	0.974
	α(H−O−H)	104.4	106.1[c], 106.3[d]	105.3	106.1	105.0
	α(Mg−O−H)	127.4	127.0[c], 126.9[d]	127.4	127.0	
	E_b	83.9 (81.9)	83.6[c](81.6[c]) 84.3[d](82.3[d])	84.8 (82.8)	85.9 (83.9)	78.4
6	r(Mg−O)	2.112	2.109[c], 2.120[d]	2.112	2.093	2.081
	r(O−H)	0.981	0.973[c], 0.976[d]	0.981	0.972	0.963
	α(H−O−H)	106.3	106.5[c], 106.4[d]	106.3	106.3	105.8
	E_b	335.3 (320.3)	320.2[c](305.2[c]) 311.4[d](296.4[d])	338.0 (323.0)	321.6 (306.6)	313.7

[a] Hexacoordinated isomer, T_h symmetry. Energies in kcal/mol, distances in angstroms, angles in degrees. [b] Values in parentheses include ZPE corrections at 298 K. [c] CP2K calculation with PBE functional. [d] CP2K calculation with BLYP functional. [e] Reference 25, MP2(FULL)/6-311++G(3df,3pd) calculation.

TABLE 3: Geometries and Hydrate Binding Energies of $Ca(H_2O)^{2+}$ and $Ca(H_2O)_6^{2+}$ [a]

$Ca(H_2O)_n^{2+}$		DGauss[b]	CPMD[b]	CPMD/BLYP[c]	B3LYP[d]	MP2
1	r(Ca−O)	2.220	2.186	2.214	2.26	2.27[e], 2.297[f]
	r(O−H)	0.993	0.983	0.986		0.962[f]
	α(H−O−H)	104.0	104.5	104.2		104.1[f]
	α(Ca−O−H)	128.0	127.8			
	E_b	63.7 (61.9)	61.2 (59.4)	58.8	56.9	58.0[e], 53.5[f]
6	r(Ca−O)	2.403	2.375	2.421	2.37	2.39[e], 2.439[f]
	r(O−H)	0.981	0.973	0.976		0.954[f]
	α(H−O−H)	105.2	105.1	105.1		105.8[f]
	E_b	241.0 (228.2)	249.0 (236.2)	240.1	234.4	257.2[e], 238.3[f]

[a] Hexacoordinated isomer, T_h symmetry. Energies in kcal/mol, distances in angstroms, angles in degrees. [b] Values in parentheses include ZPE corrections at 298 K. [c] Reference 26. [d] Reference 28, 6-311+G(2d,2p) basis set. [e] Reference 27, 6-31+G* basis set. [f] Reference 31, 6-31+G* (H and O) and (5s4p)/[3s2p] (Ca) basis sets.

TABLE 4: Properties of $Na(H_2O)_n^+$, $Mg(H_2O)_n^{2+}$, and $Ca(H_2O)_n^{2+}$ Clusters ($n = 4-7$)[a]

	isomer	symmetry	E_b [b]	ΔE[b]	d(M−O)	q(M)
Na	4	S_4	78.3 (71.5) [73.4][c]	14.5 (13.1) [13.8][c]	2.29(1)	0.67
	5A	C_{2v}	88.9		2.28−2.45	0.72
	5B	C_2	92.7 (82.7) [85.7][c]	14.4 (11.2) [12.3][c]	2.28−2.30	0.70
	5C	C_1	88.9		2.28−2.44	0.72
	6B	S_6	101.9 (88.3)		2.41(4)	0.67
	6C	D_{2d}	106.6 (93.8) [96.4][c]	13.9 (11.1) [10.7][c]	2.29(0)	0.69
	6D	C_1	101.0		2.27−2.50	0.69
	6F	C_1	103.2		2.29−2.48	0.71
	7C	C_2	115.7 (98.8)	9.1 (5.9)	2.30−2.51	0.69
	7D	C_1	114.1		2.28−2.64	0.65
Mg	4	S_4	264.2 (254.6)	46.1 (43.5)	1.99(0)	1.28
	5A	C_{2v}	294.2 (281.7)	30.0 (27.0) [26.3][d]	2.02−2.09	1.30
	5B	C_2	292.2		1.97−1.99	1.30
	6A	T_h	321.6 (306.7)	27.5 (25.0) [24.2][d]	2.09(3)	1.26
	6C	D_{2d}	320.7		1.97(7)	1.26
	6E	C_s	317.5		2.01−2.10	1.28
	7B	C_s	343.7 (326.2)	22.0 (19.5) [18.7][d]	2.07−2.11	1.23
Ca	4	S_4	193.5 (185.0)	37.6 (34.9)	2.30(2)	1.64
	5A	C_{2v}	222.7 (212.3)	29.2 (27.3) [26.7][d]	2.32−2.36	1.66
	5B	C_2	219.8		2.27−2.31	1.65
	6A	T_h	249.0 (236.2)	26.3 (23.9) [22.0][d]	2.37(5)	1.64
	6C	D_{2d}	245.4		2.28(3)	1.66
	6E	C_s	244.3		2.27−2.37	1.65
	7A	C_1	264.8		2.40−2.45	1.65
	7B	C_s	270.7 (254.8)	21.7 (18.6) [17.7][d]	2.34−2.40	1.63

[a] Energies in kcal/mol, distances in angstroms, and charges in elementary electron charge units. [b] Values in parentheses include ZPE corrections at 298 K. Experimental values are presented in square brackets. [c] Reference 36. [d] Reference 35.

experiment[36] is possible for Na^+ up to the hexamer for E_b and for most ΔE values,[35,37] and the agreement is good. The ZPE-corrected hydration energies of $Na(H_2O)_4^+$, $Na(H_2O)_5^+$, and $Na(H_2O)_6^+$ are 2−3 kcal lower than measured values, but the corresponding ΔE values are within 1 kcal/mol. The successive binding energies of divalent cations are within 1 kcal/mol of experiment, apart from $Ca(H_2O)_6^{2+}$ (1.9 kcal/mol). ΔE depends on the cluster geometry before and after H_2O removal, and this comparison is a sensitive test of the assignment of the most stable isomer. Table 2 shows that the hydration energy of $Mg(H_2O)_6^{2+}$ is close to the MP2 value,[25] and for the pentahydrate (5B) the corresponding difference is 1.9 kcal/mol. For

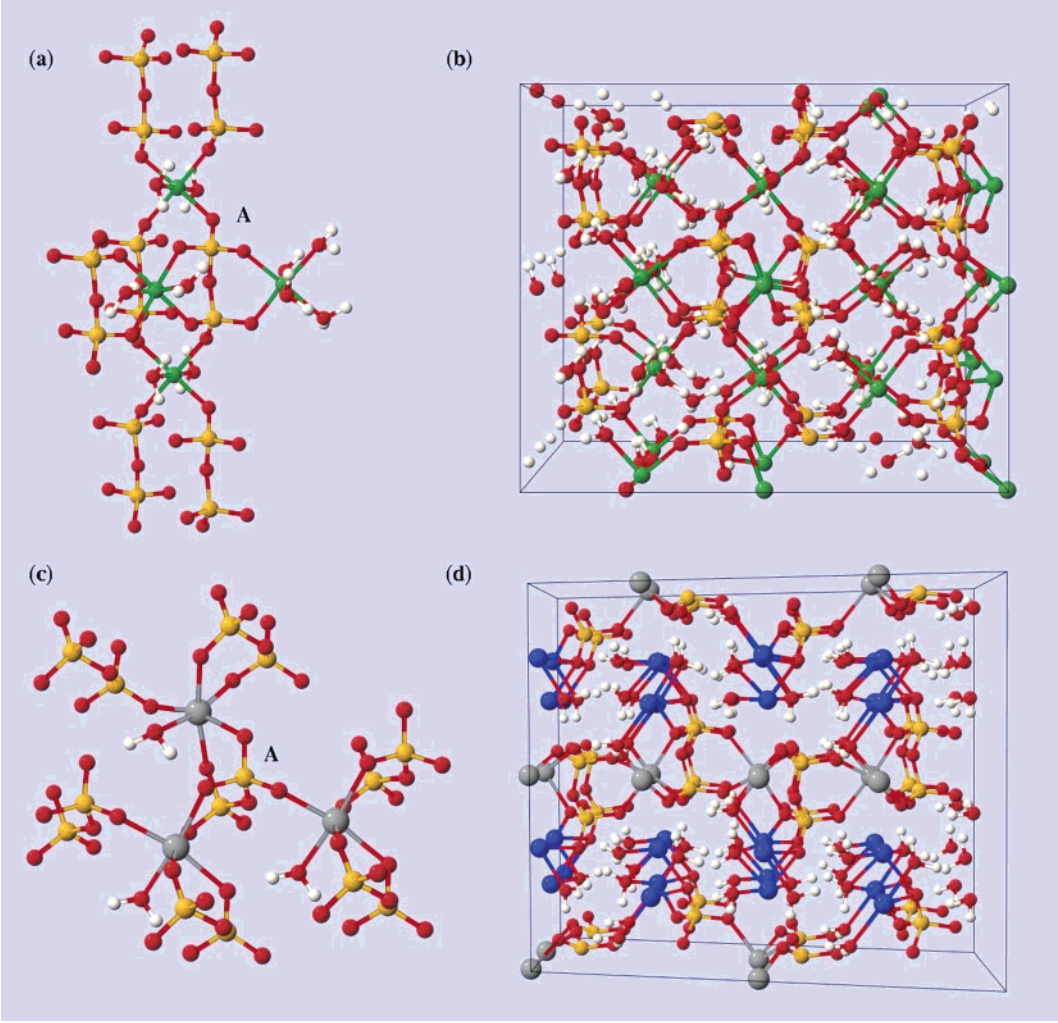

Figure 2. Structural motifs of (a and b) $Mg_2P_2O_7 \cdot 6H_2O$ ($a = 7.189$, $b = 18.309$, $c = 7.665$ Å, $\beta = 92.36°$) and (c and d) $CaNa_2P_2O_7 \cdot 4H_2O$ ($a = 5.689$, $b = 8.886$, $c = 10.565$ Å, $\beta = 106.3°$) crystals. In parts b and d both unit cells are replicated $2 \times 2 \times 2$ times.

Ca^{2+}, MP2 calculations[31] yield E_b values ($n = 4-6$) within 4 kcal/mol of our results (see the hexamer in Table 3).

The effective cation charges (Table 4) are obtained by integrating the charge density over the Wigner−Seitz cell of the cation. Electrostatic fitting leads to similar values, which vary little for different isomers and cluster sizes. Mg^{2+} has the smallest ionic radius and the largest charge transfer ($0.7-0.8e$) from the neighboring H_2O molecules. The charge transfers in Na^+ and Ca^{2+} are similar ($\geq 0.3e$), but Ca−O bonds are stronger. The B3LYP study[28] reported similar effective cation charges for the hydrates of Mg^{2+} and Ca^{2+}.

B. Mg_2 and $CaNa_2$ Pyrophosphate Crystal Salts. The structure refinement parameters (R values) of pyrophosphate compounds with varying cation and hydration contents are better than those for ATP crystals, and a comparison with DF calculations is easier. We have studied dimagnesium pyrophosphate hexahydrate ($Mg_2P_2O_7 \cdot 6H_2O$)[38] and calcium disodium pyrophosphate tetrahydrate (α-$CaNa_2P_2O_7 \cdot 4H_2O$),[39] using the CPMD program and the experimental unit cell. Both systems are monoclinic ($\beta = 92.4°$ and 106.3°, respectively) with space groups $P2_1/n$ and Pc ($Z = 4$ and 2) having 116 and 48 atoms in a unit cell (Figure 2). The experimental coordinates of Mg_2 hexahydrate include water H positions, whereas the H atoms in $CaNa_2$ tetrahydrate are placed to favor hydrogen bonding for each water molecule. This choice of hydrogen-bond network is not unique, and the experimental positions of O atoms in water show the largest mean-square displacements (temperature factors) among non-hydrogen atoms in both crystals.

The optimized structures (Figure 2) show a pyrophosphate group (A) and Mg/Ca-linked molecules (Figures 2a and 2c).[40] The divalent cations prefer octahedral coordination, there are monodentate and bidentate chelate bonds between pyrophosphates and cations, and group A is linked to six other pyrophosphates. The Mg_2 hexahydrate involves three types of Mg cations: (1) a dihydrate and four pyrophosphate groups that form two parallel vertical chains, (2) a dihydrate that makes two bidentate chelates with pyrophosphates in the perpendicular direction, and (3) a tetrahydrate with contact to A alone. The Mg_2 hexahydrate crystal structure (Figure 2b) can be described as (vertical) slabs of Mg-linked pyrophosphate chains interlocked via the Mg tetrahydrate groups (third Mg^{2+}). Hydrogen bonding of these tetrahydrate groups is not optimal, and electrostatic interaction is a major source of crystal cohesion. The $CaNa_2$ tetrahydrate crystal (Figures 2c and 2d) consists of parallel rows of Ca^{2+} and pyrophosphates, where the pyrophosphate orientations alternate. Ca cations form an octahedrally coordinated monohydrate with one monodentate and two bidentate chelates. Group A is linked via three Ca^{2+} to six neighboring pyrophosphates (Figure 2c). The Ca cations connect pyrophosphates in a direction nearly perpendicular to the P−P axis, forming corrugated layers of Ca pyrophosphate with interlayer water and Na cations. Each monomer makes four

TABLE 5: Bond Distances, Angles, and Phosphate Projection Angle in Pyrophosphate Crystal Salts[a]

	$Mg_2P_2O_7{\cdot}6H_2O$	expt[b]	$CaNa_2P_2O_7{\cdot}4H_2O$	expt[c]
P−O	1.525−1.549	1.493−1.522	1.531−1.547	1.503−1.519
P−O_s	1.641−1.643	1.620	1.625−1.656	1.622−1.641
O−H	0.976−1.003		0.978−0.997	
Na−O			2.332−2.495	2.356−2.443
Ca−O			2.308−2.432	2.313−2.407
Mg−O	2.045−2.145	2.034−2.130		
O−P−O	111.9−115.5	111.8−115.5	110.6−115.0	110.6−115.3
O−P−O_s	101.3−107.6	102.8−107.1	101.2−108.4	101.5−108.2
P−O_s−P	124.8	125.6	128.3	128.7
H−O−H	104.1−108.5		106.4−107.6	
Proj1	18.4−19.1	17.4−17.8	19.0−21.5	9.1−11.3

[a] Distances in angstroms, angles in degrees. [b] Reference 38. [c] Reference 39.

additional Na−O contacts. This structure is similar to the other known polymorph of $CaNa_2$ tetrahydrate (β-form) with parallel Ca^{2+} and $P_2O_7^{4-}$ chains, but the Na^+ and H_2O coordinations differ.[41]

The structural parameters of Mg_2 hexahydrate and $CaNa_2$ tetrahydrate (Table 5) show that P−O and P−O_s bonds (O_s denotes a bridging oxygen) are slightly (<2%) longer than measured values but typical for pyrophosphate anions.[42,43] The range of Mg−O distances and their average value (2.095 Å) are close to those measured (average value 2.085 Å), and this also holds for the Ca^{2+} ion (average values 2.371 and 2.347 Å, respectively). Both Na^+ coordination polyhedra are distorted octahedra, with one Na−O ligand significantly longer than the others (∼2.8 Å, omitted from Table 5). The range of Na−O distances and their average value 2.407 Å are similar to those measured (average value 2.403 Å). The covalent O−H bonds are reported only for the calculations due to the limited experimental accuracy (see above). The variation in bond lengths is caused by hydrogen bonding.

The calculated bond angles (Table 5) are close to measured values for both terminal and bridging O atoms, with P−O_s−P angles within 1° of those measured. Small values of these angles had been regarded as an effect of cation-induced strain and a probable reason for the hydrolytic activity of divalent cations. Our earlier study showed, however, that the P−O_s−P bridges of solvated methyl triphosphate have small angles with and without a bidentate chelate configuration with Mg^{2+}.[4] The projection angles (Proj1) defined via O−P···P−O correspond to a nearly eclipsed phosphate conformation and differ for the two structures: The angle for Mg_2 hexahydrate is very similar to the experimental value, whereas it increases by 10° during optimization in the case of $CaNa_2$ tetrahydrate. This change is linked to the Na^+ coordination, where the longest oxygen ligand shrinks/increases by 0.1 Å for the two types of Na^+ present.

The vibrational densities of states (vDOS) of the two pyrophosphate crystal salts are shown in Figure 3. The frequencies above 3100 cm^{-1} are O−H stretching modes of water molecules, and the different red shifts for Mg_2 hexahydrate and $CaNa_2$ tetrahydrate reflect differences in local hydrogen bonding. The peak at 1560−1650 cm^{-1} (1590−1640 cm^{-1}, H−O−H bending) is slightly broader for the system containing Mg^{2+}. The P−O stretching frequencies of $P_2O_7^{4-}$ start at 1150 cm^{-1} (1130 cm^{-1}), and symmetric PO_4^{2-} breathing modes occur at 960 cm^{-1} (950−990 cm^{-1}), with P−O_s stretching modes at 890 cm^{-1} in both crystals. The experimental infrared spectra[9] of ternary complexes of ATP, bis(2-pyridyl)amine, and divalent cations show P−O and P−O_s stretching frequencies at 1235 and 895 cm^{-1}, respectively. The slight shift in the P−O stretch arises from the negative charge of P_2O_7,$^{4-}$ which is distributed over more oxygen atoms in the case of the ATP triphosphate tail. Analysis of the lower frequency modes is complicated, but a P−O_s−P bridge bending mode is found at 600 cm^{-1} for Mg_2 hexahydrate and at 570 and 700 cm^{-1} for $CaNa_2$ tetrahydrate. The cation−oxygen stretching modes are in the ranges 380−430 cm^{-1} (Mg^{2+}), 300−340 cm^{-1} (Ca^{2+}), and 270−340 cm^{-1} (Na^+).

C. Crystal Structure of Na_2ATP Trihydrate. *1. Experimental Situation.* The original X-ray analyses of Na_2ATP trihydrate[11,12] led to an orthorhombic unit cell with space group $P2_12_12_1$ (Figure 4); eight ATP monomers (types A and B, Chart 1) form asymmetric dimers linked by hydrogen bonds and Na^+ ligands (Figure 5). The dimers are interlocked along the *c*-axis, and the helically folded triphosphate tails couple the same type of monomers via Na^+ ions (sites Na1 and Na2) and hydrogen bonds (O_α−H_γ). Two of the four crystallographically distinct Na^+ sites involve an octahedral coordination of Na^+ with the triphosphate chains and adenine nitrogen atoms, and the others are penta- and hexacoordinated, respectively, with O atoms in water, ribose, and phosphate. The last two Na^+ ions (Na3 and Na4) link blocks of ATP dimers with water channels between them, and the existence of two crystal structures implies mobility of the cations and water molecules.[12,13]

Humidity-controlled single-crystal measurements[13,44,45] confirm that these motifs prevail as the water content increases from monohydrate to trihydrate. This reversible transition is accompanied by a linear change in one cell parameter. High-resolution NMR measurements[45] show an alternation in one ribose group (type B) with changing hydration. The crystal structures of Na_2ATP di- and trihydrate[13] indicate that dehydration is accompanied by a loss of water molecules near the ribose groups.

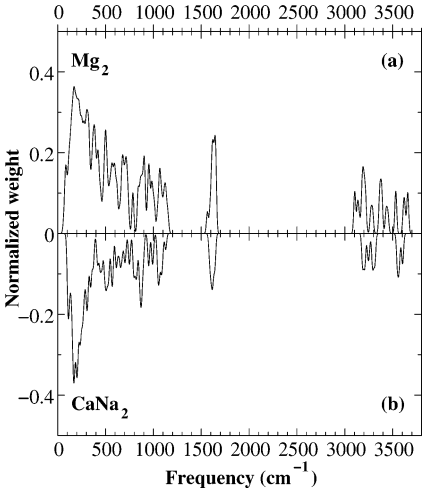

Figure 3. Calculated vibrational density of states of (a) $Mg_2P_2O_7{\cdot}6H_2O$ and (b) $CaNa_2P_2O_7{\cdot}4H_2O$ crystals. A Gaussian broadening of 10 cm^{-1} has been used.

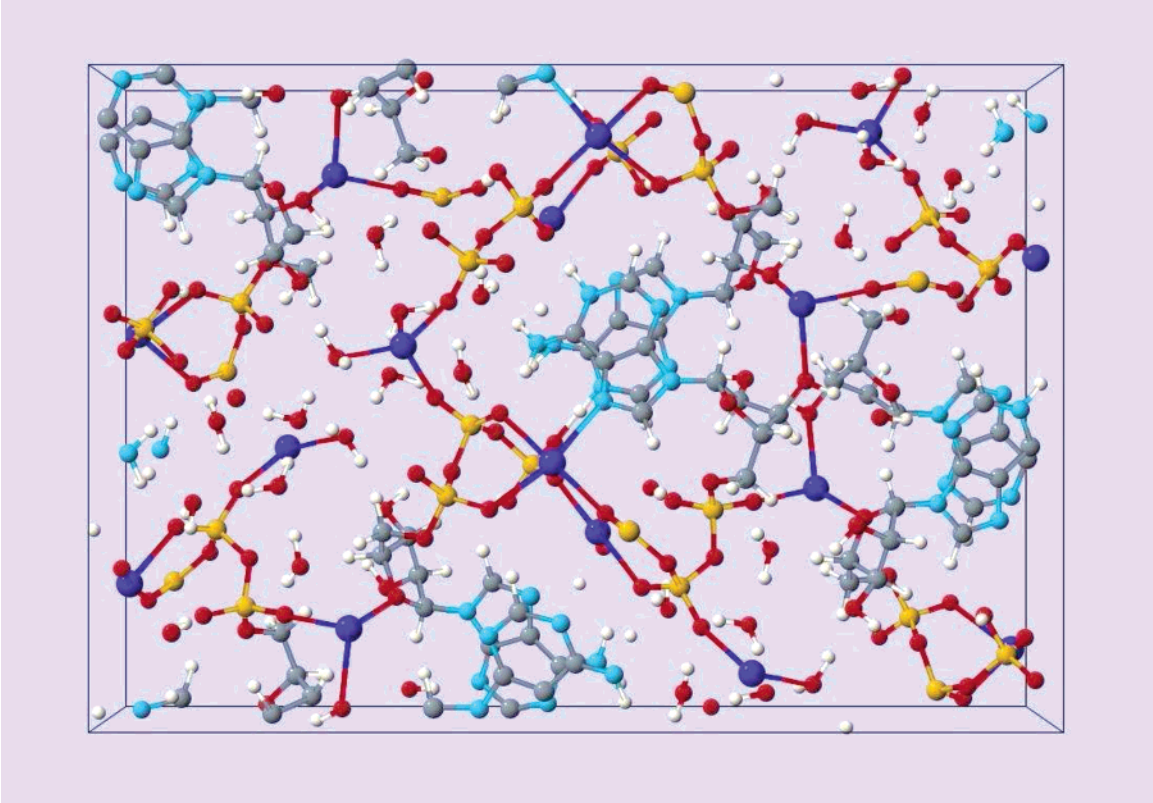

Figure 4. Orthorhombic unit cell of Na_2ATP trihydrate. There are eight ATP monomers, 16 Na^+ ions, and 24 water molecules with the $P2_12_12_1$ space group ($Z = 4$). The structure is optimized with a DF method. ATP monomers appear cut because of the unit cell boundaries ($a = 30.45$, $b = 20.88$, $c = 7.07$ Å).

CHART 1: $H_2(ATP)^{2-}$ Molecule

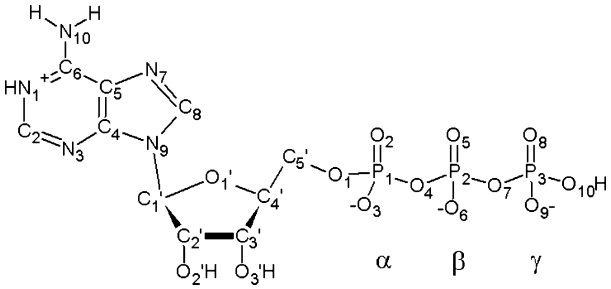

The ATP dimer complexed with cations Na1 and Na2 is shown in Figure 5.[46] Salt bridges (Na−O) shorter than 2.7 Å are plotted as solid lines (Figure 5a, optimized structure); longer bridges and hydrogen bonds between adenine and phosphate are dashed. The structure shows encapsulated Na cations that are octahedrally coordinated by the phosphate O atoms and adenine N atoms as well as by the O_γ from the upper/lower-lying dimer. The phosphate tails are arranged helically along the *c*-axis with hydrogen bonds to the α-phosphates of neighboring dimers. Both triphosphates form a tridentate chelate with Na^+, but the linkage with O_α is slightly weaker for monomer A. The Na−N ligand coordinating the adenine group of monomer B is expanded significantly, and experimental values for ionic contacts vary between 2.44−2.99 Å and 2.30−2.64 Å for Na1 and Na2, respectively. There are significant deviations from perfect octahedral coordinations for both cations.

ATP hydrates with divalent cations Mg^{2+} and Ca^{2+} (other than ternary complexes)[9] cannot be crystallized, since the phosphate group is unstable toward hydrolysis. The cation charge affects ATP protonation, which differs in Na_2ATP hydrate (ATP charge −2, base protonated) from that in biological environments (ATP charge −4, base neutral). This is based on the fact that ATP exists mainly in its deprotonated form at pH 7 as the pK_a value corresponding to fourth proton removal is 6.5.[47−49] The adenine pK_a value is 3.8 under normal solvent conditions, indicating that the N1 site should be deprotonated. However, this property is environment-dependent and can be modified as in 23S ribosomal RNA, where adenine has a near-neutral pK_a (7.6) and catalyzes peptide bond formation.[50]

2. Calculations. The initial structure was constructed from several sources, including the experimental crystal structure.[12] The aliphatic H atoms in ATP were taken from the structure of the free molecule,[4] and plausible hydrogen bond acceptor−donor pairs determined the orientation for hydroxyl and amine groups. The location of water molecules is complicated, since the oxygen positions in the crystal do not satisfy perfect hydrogen bonding. Furthermore, H_2O and Na^+ contain the same number of valence electrons and can easily be confused in X-ray measurements. In fact, Sugawara et al.[13] suggested that one Na^+ (Na4) should be interchanged with a water molecule (OW4).

We have used the original H_2O oxygen positions[12] and introduced H atoms to satisfy the requirements of molecular geometry and optimal hydrogen bonding. Four test structures were optimized in short DF simulations, and the final system (448 atoms) was optimized in a fixed unit cell using simulated annealing with a plane wave cutoff of 80 Ry. There were significant changes in the water channels during optimization, and the final structure is shown in Figure 4. The labeling of atoms in the $H_2(ATP)^{2-}$ molecule is shown in Chart 1.

The dimer configurations for the optimized and experimental structures are shown in Figure 5b. The agreement is good, with some deviations in the ribose group location and adenine base orientation of monomer A (see below). The Na cations are shifted slightly but maintain their separation (3.53 Å). There

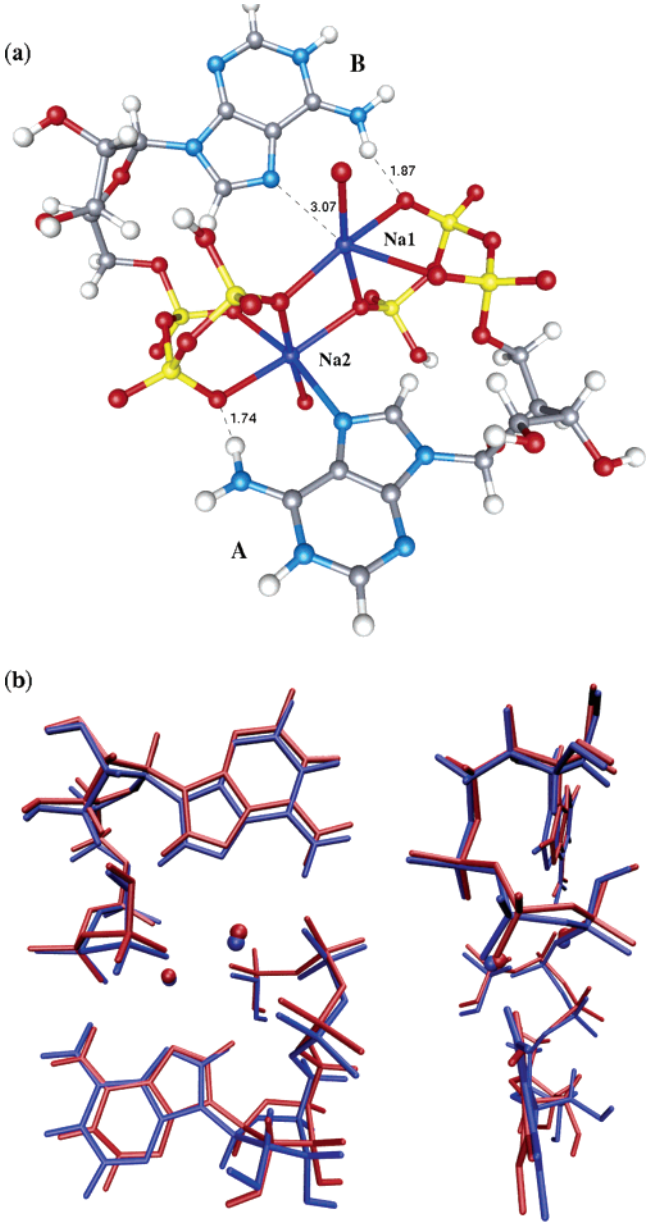

Figure 5. (a) ATP dimer in the optimized crystal structure and (b) comparison between the experimental and the theoretical ATP dimer conformations: red, experiment; blue, DF-optimized structure.

are no significant changes in the Na coordination; the average ligand distances are 2.45 (2.47) Å and 2.60 (2.57) Å for experiment (theory), and the longer Na−N contacts are 2.99 (3.07) Å and 2.64 (2.65) Å for the cations Na1 and Na2, respectively. The acceptor−donor distances between O_β and amine N (O6−N10) are little changed (2.78 (2.78) Å and 2.80 (2.87) Å, respectively).

The protonated adenine groups form hydrogen bonds with the terminal phosphate groups in neighboring dimers (N1) and with water molecules (N10). An unusually long N−H distance (1.13 Å) is observed between the acceptor−donor pair O9B−N1B′. The bond distances in the adenine base differ from experiment by an average of 0.017 Å, and the average bond lengths are slightly (0.005 Å) larger for DF calculations. The structure of the free ATP molecule (base neutral) agrees better with experiment (average bond distance and deviation of 0.002 and 0.007 Å, respectively), and the protonation of N1 leads to deviations of up to 0.03 Å within the heterocyclic ring. The C6−N10 distance for amine nitrogen atoms is shorter (1.32 Å) than that in experiment and in free ATP (1.35 Å), which can be related to the hydrogen bonding of the amine groups. The adenine bases are anti according to the glycosidic angles (Table 6), which agrees well with experiment. The difference of 10.7° for type A is related to the change in the ribose structure.

TABLE 6: Conformational Parameters of the Adenosine Part of ATP in Degrees: Torsional Angles around the Glycocidic C1′−N9 Bond (χ), C4′−C5′ Bond (ψ), and C5′−O1 Bond (ϕ), and the Pseudorotation Angle (P) of the Ribose Ring

	ATP[a]	crystal (A/B)	EXP1 (A/B)[b]	EXP2 (A/B)[c]
χ	27.2	−9.2/−22.5	1.5/−17.7	−4.2/28.4
ϕ	46.3	−61.8/−70.7	−61.0/−64.7	56.5/56.2
ψ	−99.6	116.4/136.4	142.4/138.4	−140.6/−139.0
P	34	8/174	−5/182	177/5

[a] Density functional calculation from ref 4. [b] Reference 12. [c] Reference 13.

The ribose groups participate in hydrogen bonding via contacts between their hydroxyl side groups, with water molecules, and with N3B′ from the overlying adenine base. In addition, the hydroxyl oxygen atoms O1′B, O2′B, and O3′A form ligands with the pentacoordinated Na4. The formation of a hydrogen bond between O2′A and N3B′ is coupled with a significant change in the ribose conformation during optimization; Na3 has a ligand with O2′A in the experimental structure, and this is replaced by H_2O as the hydroxyl group moves along the *c*-axis toward N3B′. This displacement is reflected in the glycosidic angle of the adenine base and in the torsional angle around the C5′−O1 bond (Table 6). The sugar puckering angles (pseudorotation angles)[51] corresponding to C2′-endo-C3′-exo (A) and C2′-exo-C3′-endo (B) agree well with experiment for both monomer types. The torsions around the C4′−C5′ bonds are gauche(−). The adenosine conformations differ (Table 6), because the measured ATP molecules[13] are different optical enantiomers. The sign of the torsion angles in the triphosphate tail (Table 7) is also reversed.

The bonds in the ribose group are 0.010 Å longer on average than measured values, and the C5′−O1 ester bond is 0.03 Å longer (1.45 Å, Table 7) than those in experiment in both types of ATP. For the free ATP molecule, the ribose ring conformation reduces the overall agreement with experiment slightly, and the C5′−O1 ester bond differs by 0.06 Å.

The structural parameters of triphosphate tails are listed in Table 7. The calculated triphosphate bond distances are longer than those measured on average by 0.030 Å (or 0.040 Å).[13] This is evident in the P3−O7 (monomer A) and P3−O10 bonds (both monomers), where the first corresponds to the terminal bridging anhydride bond ($P_\gamma-O_s$) and the latter involves a nonbridging oxygen in a protonated state. The Na1 and Na2 cations form tridentate chelates with the three phosphate groups of neighboring ATP, leading to weaker covalent P−O bonds, particularly those involved in $P-O_s-P$ bridges. The effect is enhanced in group A for P3−O7, where the Na1−O2 (α-phosphate) ligand is relatively long (2.68 Å) and the Na1−triphosphate complex resembles a bidentate chelate. The (experimental) starting structure shows smaller fluctuations in the bond lengths.

The anhydride bridge angles in Table 7 are slightly smaller than the experimental values. The magnitude of the $P-O_s-P$ angles (<140°) suggests little cation-induced strain, and this is apparent in our DF study for Mg^{2+}-complexed methyl triphosphate in water,[4] where the $P-O_s-P$ angle fluctuates around 128° with and without the cation. The torsional angles around anhydride bonds agree satisfactorily for type A, but ω_1', ω_2,

TABLE 7: Bond Distances, Angles, and Torsional Angles of Triphosphate in $Na_2ATP{\cdot}3H_2O$ Crystal Salt and Torsional Angles around Bridging O1−P1 (ω_1), P1−O4 (ω_1'), O4−P2 (ω_2), and P2−O7 (ω_2') Bonds[a]

	Na (A/B)	EXP1 (A/B)[b]	EXP2 (A/B)[c]	Mg (A)[d]	Ca (A)[d]
C5′−O1	1.446/1.448	1.418/1.419	1.455/1.433	1.438	1.440
P1−O1	1.621/1.627	1.570/1.638	1.584/1.612	1.609	1.615
P1−O2	1.513/1.522	1.502/1.482	1.473/1.468	1.516	1.510
P1−O3	1.519/1.506	1.503/1.491	1.446/1.485	1.515	1.517
P1−O4	1.633/1.636	1.602/1.599	1.600/1.616	1.639	1.642
P2−O4	1.644/1.640	1.629/1.623	1.607/1.560	1.645	1.641
P2−O5	1.504/1.492	1.502/1.514	1.495/1.479	1.504	1.505
P2−O6	1.523/1.529	1.495/1.490	1.456/1.492	1.550	1.541
P2−O7	1.628/1.620	1.581/1.607	1.599/1.577	1.595	1.603
P3−O7	1.686/1.647	1.609/1.628	1.630/1.581	1.756	1.740
P3−O8	1.502/1.508	1.486/1.488	1.467/1.478	1.549	1.536
P3−O9	1.529/1.539	1.485/1.489	1.501/1.484	1.554	1.571
P3−O10	1.594/1.588	1.510/1.503	1.566/1.539	1.499	1.502
C5′−O1−P1	123.7/116.3	123.9/121.8	121.5/120.1	129.1	127.2
P1−O4−P2	130.9/128.5	134.0/134.5	131.8/134.1	125.2	126.3
P2−O7−P3	137.3/132.5	140.5/137.6	134.2/138.6	135.4	137.9
ω_1	67.9/−66.6	54.9/−66.2	−44.5/71.7	62.3	64.8
ω_1'	71.1/176.2	69.2/−153.4	−76.2/151.9	77.1	75.0
ω_2	−63.1/141.6	−51.3/115.8	61.5/−116.5	−63.6	−61.2
ω_2'	101.4/−53.2	113.5/−82.6	−117.6/88.2	97.7	99.5
Proj1	14.2/−42.4	20.5/−35.5	−20.5/36.8	20.5	20.2
Proj2	−31.6/31.3	−33.0/32.4	36.9/−35.9	−13.9	−15.6

[a] Distances in angstroms, angles in degrees. [b] Reference 12. [c] Reference 13. [d] Substitution of one Na1 and removal of a proton at O10.

and ω_2' of type B differ by ∼30° from experiment. Much smaller deviations are observed in the O−P···P−O projection angles describing the orientation of phosphate groups. No conformation is eclipsed (0°) or staggered (60°), and close agreement with the experiment is found for the β- and γ-phosphate orientations (Proj2).

The dipole moments of individual water molecules and ATP monomers have been calculated using localized Wannier orbitals.[52] The average water dipole moment (3.2 D, with a range 2.9−3.5 D) is slightly larger than that of bulk water calculated using the same procedure.[53] Analysis of the local environment of OW5 shows that its large dipole moment (3.5 D) correlates with the strong binding with Na3 (2.32 Å) as well as with effective hydrogen bonding. Similarly, OW2 participates only in hydrogen bonding resulting in the lower limit (2.9 D) for dipole moment. The positively (adenine) and negatively (triphosphate) charged ends of ATP monomers (net charge −2) cause large dipole moments of 119.6 and 117.6 D for types A and B, respectively. Assuming that the crystal consists of ATP dimers, we have also calculated the net dipole moment of this configuration with two additional Na cations (Na1 and Na2). The asymmetry of the dimer combined with the negative net charge of −2 yields a large dipole moment (65.5 D), which is approximately parallel to the *b*-axis (angle 29.2°). Taking into account the $P2_12_12_1$ space group, a picture emerges where the crystal comprises slices of opposing dipoles.

Divalent cations enhance hydrolysis in ATP, and we have studied their interactions with the triphosphate part of ATP by substituting Mg^{2+} and Ca^{2+} for one of four crystallographically identical cations (Na1, $Z = 4$). Neutrality is maintained by removing one proton attached to the terminal phosphate oxygen (O10) of the type A ATP monomer involved, and the asymmetric units of ATP dimers are shown in Figure 6. An obvious difference from the initial structure with Na1 is seen for Mg^{2+} coordination: The smaller ionic radius of Mg^{2+} results in a contraction of four Mg−O ligands (2.01−2.09 Å, Figure 6a) within the dimeric unit, where the tetracoordinated Mg cation forms a tight tridentate chelate conformation with the triphosphate tail of monomer A. The initial contacts with the adenine base (3.50 Å, monomer B) and the neighboring ATP dimer above (2.80 Å, monomer A) have increased. However, the

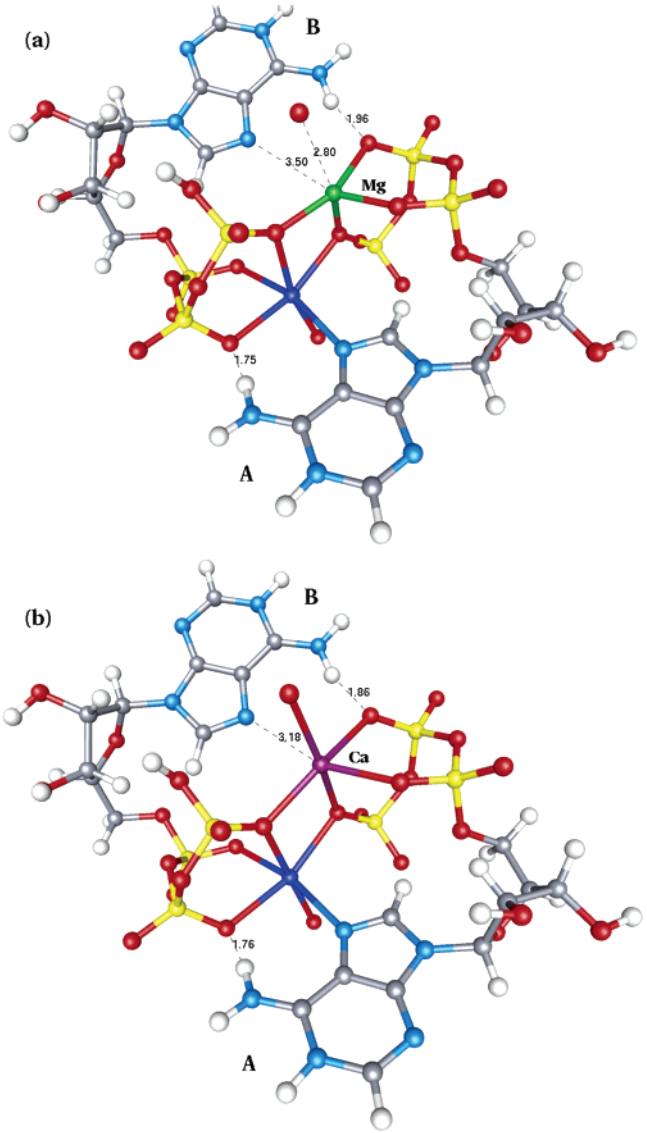

Figure 6. ATP dimer in the optimized crystal structure with (a) Mg^{2+} substitution, and (b) Ca^{2+} substitution.

optimized structure for Ca^{2+} (Figure 6b) differs little from the starting configuration (the ionic radii of Na^+ and Ca^{2+} are very similar), and the Ca cation remains hexacoordinated. The resulting scatter for Ca−O ligands (2.30−2.46 Å) is smaller than that for Na1 due to the stronger bonding in the former. The effect of Na1 substitution on the coordination of neighboring Na2 is very small in both cases.

The structural parameters (Table 7) show cation-induced changes in the triphosphate tail. As observed for the pyrophosphate crystal salts (section III.B), the complexation with divalent cations increases the length of nonbridging P−O bonds. The effect is even larger for the terminal bridging P3−O7 bond, which increases to 1.76 and 1.74 Å for Mg^{2+} and Ca^{2+}, respectively, and is compensated slightly by a contraction of the P2−O7 bond. The anhydride bond and torsional angles are similar to the initial unsubstituted case, and this is also true for the projection angle between α- and *β*-phosphates. The second projection angle (Proj2) shows a decrease of over 15° on the eclipsed side, due to the deprotonation of the terminal phosphate.

Effective charges of 0.66*e* and 0.63*e* are found for the hexacoordinated Na1 and Na2, respectively, in the unsubstituted structure. The four salt bridges of Na3 with water and *β*-phosphates result in a smaller charge transfer (effective charge 0.75*e*), while the value for pentacoordinated Na4 (0.67*e*) is close to the above. Na1 substitution by Mg and Ca leads to a charge transfer of 0.76*e* for Mg (effective charge 1.24*e*), whereas the charge attracted for Ca (effective charge 1.58*e*) differs little from that of Na1.

IV. Discussion and Concluding Remarks

Adenosine 5′-triphosphate (ATP) is essential to cellular metabolism and has been studied intensely for decades. Computer hardware and algorithmic developments in recent years have made possible the calculation of structures and energy differences in ATP-related systems using methods that are free of adjustable parameters. We have applied density functional methods here to molecular systems related to ATP, with the aim of providing benchmarks for their application in biological reactions. An example is provided in the companion paper by the hydrolysis of ATP in the presence of the active site in the protein actin.

The applicability of DF method was tested first for the $Na(H_2O)_n^+$, $Mg(H_2O)_n^{2+}$, and $Ca(H_2O)_n^{2+}$ clusters ($n = 1, 4-7$) as well as for the Mg_2 and $CaNa_2$ pyrophosphate crystal salts. The simulations produce accurate cation−oxygen distances for both the hydrate clusters and pyrophosphate crystals, and the water binding energies (clusters) agree well with experimental results and other quantum chemical calculations. The structure of pyrophosphate units is reproduced well, especially for the $Mg_2P_2O_7 \cdot 6H_2O$ crystal, where the experimental data include the locations of hydrogen atoms. The DF structures for pyrophosphates are reliable, and the calculations are well-converged in terms of the plane wave basis set (100 Ry). Nonbridging P−O bonds are sensitive to the local environment (cations, hydrogen bonds), and length changes of few percent can occur.

The crystal structure of Na_2ATP trihydrate has been optimized, starting from the experimental X-ray result and adding missing H atoms. The crystal environment differs significantly from aqueous solutions or a protein active site, and the ATP monomer has a double-protonated form ($H_2(ATP)^{2-}$) with a positive (protonated) adenine base and a negative hydrophilic phosphate tail. The crystal salt consists of asymmetric units of ATP dimers held together by two Na cations (Na1 and Na2), whose coordination polyhedra do not change upon optimization. The net dipole moments of ATP dimers are large (65.5 D) and are roughly parallel and antiparallel to the crystal *b*-axis. Together with the $P2_12_12_1$ space group this leads to a picture where the periodic ATP blocks have alternating dipoles along the *b*-axis. Comparison with the experimental starting structure shows good overall agreement, but there are changes in the ribose and adenine conformation of monomer A caused by the limited experimental accuracy on water oxygens and the existence of other possible forms of the hydrogen-bond network. The calculated P−O and P−O_s bonds of the triphosphate tail are longer (on average by 0.03 Å), and the bridging P−O_s bonds show marked alternations ranging from 1.62 to 1.69 Å, with the upper limit found for the terminal P−O_s bonds (P3−O7). The dipole moments of individual water molecules range between 2.9 and 3.5 D, reflecting differences in local environment (Na coordination, hydrogen bonding).

The effect of divalent cation substitution has been studied by replacing one Na^+ (Na1) by Mg^{2+} or Ca^{2+}. The small ionic radius of Mg^{2+} results in a tetracoordinated cation with 0.3−0.4 Å shorter cation−oxygen distances, but the distorted octahedral coordination is preserved for Ca^{2+}. Despite differences in coordination, both cations lead to longer terminal P−O_s bonds (up to 1.74−1.76 Å), indicating an increased affinity for hydrolysis. The calculated effective charges (cation−hydrate clusters and ATP crystals) show that Mg^{2+} is strongly electrophilic, capturing 0.7−0.8 electrons from the nearby O atoms and that the negatively charged triphosphate tail must donate additional charge in the absence of water. This may contribute to the spontaneous hydrolysis of Mg^{2+}−ATP under crystal growing conditions.

Of particular importance for the application to larger systems is the sensitivity of the calculation scheme to choice of basis set and exchange−correlation energy functional and, of course, to its ability to reproduce available experimental results. We find that extensive basis sets are essential in the context of pyrophosphate and ATP crystal salts and that the water molecules appear the most sensitive components. For localized basis sets, marked differences can be observed between DZVP and QZV3P, and additional test calculations indicate that a TZV2P basis is adequate in terms of convergence. For a plane wave basis set and Troullier−Martins pseudopotentials, a kinetic energy cutoff of 80 Ry is satisfactory, although slight changes in H_2O geometry and orientation were observed when the calculations are repeated for 100 Ry. Comparison with all-electron calculations shows that the pseudopotential approximation performs well when the semicore electrons are included explicitly in the metal cation valence. Our experience with generalized gradient approximation (GGA) functionals indicates that PBE performs slightly better than BLYP for isolated metal cation hydrates. Extensive studies of liquid water at 300 K show that the two are equivalent in terms of structure and dynamics and that there is room for improvement.[54]

Acknowledgment. The calculations were performed on the IBM p690 supercomputer (JUMP) and the Cray SV1ex computer in the Forschungszentrum Jülich with grants of computer time from the Forschungszentrum and the John von Neumann Institute for Computing. We thank M. Krack and M. Parrinello (ETH Zürich) for support and helpful discussions and Y. Sugawara (Kitasato University) for providing the coordinates of the Na_2ATP trihydrate crystal.

References and Notes

(1) Devlin, T. M. *Textbook of Biochemistry with Clinical Correlations*, 4th ed.; Wiley-Liss: New York, 1997.

(2) Boyer, P. D. *Nobel Lectures, Chemistry 1996−2000*; Grenthe, I., Ed.; World Scientific Publishing: Singapore, 2003; p 120.

(3) Singleton, M. R.; Wigley, D. B. *EMBO J.* **2003**, *22*, 4579.

(4) Akola, J.; Jones, R. O. *J. Phys. Chem. B* **2003**, *107*, 11774.

(5) Ballone, P.; Jones, R. O.; Akola, J., to be submitted for publication.

(6) CPMD program version 3.7, Hutter, J. et al., Max-Planck-Institut für Festkörperforschung and IBM Research 1990−2003.

(7) Orioli, P.; Cini, R.; Donati, D.; Mangani, S. *J. Am. Chem. Soc.* **1981**, *103*, 4446.

(8) Sheldrick, W. S. *Z. Naturforsch., B: Chem. Sci.* **1982**, *37*, 863.

(9) Cini, R.; Burla, M. C.; Nunzi, A.; Polidori, P. G.; Zanazzi, P. *J. Chem. Soc., Dalton Trans.* **1984**, 2467.

(10) Sabat, M.; Cini, R.; Haromy, T.; Sundaralingam M. *Biochemistry* **1985**, *24*, 7827.

(11) Kennard, O.; Isaacs, N. W.; Motherwell, W. D. S.; Coppola, J. C.; Wampler, D. L.; Larson, A. C.; Watson, D. G. *Proc. R. Soc. London, Ser. A* **1971**, *325*, 401.

(12) Larson, A. C. *Acta Crystallogr., Sect. B* **1978**, *34*, 3601.

(13) Sugawara, Y.; Kamiya, N.; Iwasaki, H.; Ito, T.; Satow, Y. *J. Am. Chem. Soc.* **1991**, *113*, 5440.

(14) Troullier, N.; Martins, J. L. *Phys. Rev. B* **1991**, *43*, 1993.

(15) Perdew, J. P.; Burke, K.; Ernzerhof, M. *Phys. Rev. Lett.* **1996**, *77*, 3865.

(16) CP2K Developers Group: 2000−2004. http://cp2k.berlios.de.

(17) Goedecker, S.; Teter, M.; Hutter J. *Phys. Rev. B* **1996**, *54*, 1703.

(18) Lippert, G.; Hutter, J.; Parrinello, M. *Mol. Phys.* **1997**, *92*, 477.

(19) Becke, A. D. *Phys. Rev. A* **1988**, *38*, 3098.

(20) Lee, C.; Yang, W.; Parr R. G. *Phys. Rev. B* **1988**, *37*, 785.

(21) DGauss program, UniChem package of Oxford Molecular Group (double-ζ basis with polarization functions DZVP, auxiliary basis A1).

(22) Perdew, J. P.; Wang, Y. *Phys. Rev. B* **1992**, *45*, 13244.

(23) Poisson equations are solved using the method of Hockney, R. W. *Methods Comput. Phys.* **1970**, *9*, 136.

(24) The BFGS procedure is described in Fletcher, R. *Practical Methods of Optimization*; Wiley: New York, 1980; Vol. 1.

(25) Markham, G. D.; Glusker, J. P.; Bock, C. W. *J. Phys. Chem. B* **2002**, *106*, 5118.

(26) Bakó, I.; Hutter, J.; Pálinkás, G. *J. Chem. Phys.* **2002**, *117*, 9838.

(27) Merrill, G. N.; Webb, S. P.; Bivin, D. B. *J. Phys. Chem. A* **2003**, *107*, 386.

(28) Pavlov, M.; Siegbahn, P. E. M.; Sandström, M. *J. Phys. Chem. A* **1998**, *102*, 219.

(29) Lee, H. M.; Tarakeshwar, P.; Park, J.; Kolaski M. R.; Yoon, Y. J.; Yi, H.-B.; Kim, W. Y.; Kim, K. S. *J. Phys. Chem. A* **2004**, *108*, 2949.

(30) Glendening, E. D.; Feller, D. *J. Phys. Chem.* **1995**, *99*, 3060.

(31) Glendening, E. D.; Feller, D. *J. Phys. Chem.* **1996**, *100*, 4790.

(32) White, J. A.; Schwegler, E.; Galli, G.; Gygi, F. *J. Chem. Phys.* **2000**, *113*, 4668.

(33) Lightstone, F. C.; Schwegler, E.; Hood, R. Q.; Gygi, F.; Galli, G. *Chem. Phys. Lett.* **2001**, *343*, 549.

(34) Vuilleumier, R.; Sprik, M. *J. Chem. Phys.* **2001**, *115*, 3454.

(35) Rodriguez-Cruz, S. E.; Jockusch, R. A.; Williams, E. R. *J. Am. Chem. Soc.* **1999**, *121*, 8898.

(36) Džidić, I.; Kebarle, P. *J. Phys. Chem.* **1970**, *74*, 1466.

(37) Peschke, M.; Blades, A. T.; Kebarle, P. *J. Phys. Chem. A* **1998**, *102*, 9978.

(38) Souhassou, M.; Lecomte, C.; Blessing, R. H. *Acta Crystallogr., Sect. B* **1992**, *48*, 370.

(39) Cheng, P.-T.; Pritzker K. P. H.; Nyburg, S. C. *Acta Crystallogr., Sect. B* **1980**, *36*, 921.

(40) Three-dimensional rotatable images in xyz-format are available (Mg2-pyro-motif.xyz, CaNa2-pyro-motif.xyz).

(41) Cheng, P.-T.; Nyburg, S. C.; Adams, M. E.; Pritzker K. P. H. *Cryst. Struct. Commun.* **1979**, *8*, 313.

(42) Mandel, N. S. *Acta Crystallogr., Sect. B* **1975**, *31*, 1730.

(43) Balić-Žunić, T.; Christoffersen, M. R.; Christoffersen, J. *Acta Crystallogr., Sect. B* **2000**, *B56*, 953.

(44) Urabe, H.; Sugawara, Y.; Kasuya, T. *Phys. Rev. B* **1995**, *51*, 5666.

(45) Shindo, Y.; Naito, A.; Tuzi, S.; Sugawara, Y.; Urabe, H.; Saito, H. *J. Mol. Struct.* **2002**, *602−603*, 389.

(46) A three-dimensional rotatable image in xyz-format is available (ATP-dimer.xyz).

(47) Irani, R. R.; Taulli, T. A. *J. Inorg. Nucl. Chem.* **1966**, *28*, 1011.

(48) Sigel H.; Tribolet, R.; Malini-Balakrishnan R.; Martin, R. B. *Inorg. Chem.* **1987**, *26*, 2149.

(49) Tribolet, R.; Sigel, H. *Eur. J. Biochem.* **1988**, *170*, 617.

(50) Muth, G. W.; Ortoleva-Donnelly, L.; Strobel, S. A. *Science* **2000**, *289*, 947.

(51) Altona, C.; Sundaralingam, M. *J. Am. Chem. Soc.* **1972**, *94*, 8205.

(52) Berghold, G.; Mundy, C. J.; Romero, A. H.; Hutter, J.; Parrinello, M. *Phys. Rev. B* **2000**, *61*, 10040.

(53) Silvestrelli, P. L.; Parrinello, M. *Phys. Rev. Lett* **1999**, *82*, 3308.

(54) VandeVondele, J.; Mohamed, F.; Krack, M.; Hutter, J.; Sprik, M.; Parrinello, M. *J. Chem. Phys.* **2005**, *122*, 014515.

(55) Wong, A.; Wu, G. *J. Phys. Chem. A* **2003**, *107*, 579.